Friction **11**(5): 820–835 (2023)
https://doi.org/10.1007/s40544-022-0698-2
ISSN 2223-7690
CN 10-1237/TH

RESEARCH ARTICLE

Does friction contribute to formability improvement using servo press?

Kali PRASAD[1,†,*], Aishwary GUPTA[2,†], Hariharan KRISHNASWAMY[1,*], Uday CHAKKINGAL[3], Dilip K. BANERJEE[4], Myoung-Gyu LEE[2]

[1] *Department of Mechanical Engineering, Indian Institute of Technology Madras, Chennai 600036, India*

[2] *Department of Materials Science and Engineering, Seoul National University, Seoul 08826, Republic of Korea*

[3] *Department of Metallurgical and Materials Engineering, Indian Institute of Technology Madras, Chennai 600036, India*

[4] *Material Measurement Laboratory, National Institute of Standards and Technology (NIST), Gaithersburg 20899, USA*

Received: 08 March 2022 / Revised: 03 May 2022 / Accepted: 21 September 2022

Abstract: Servo press forming machines are advanced forming systems that are capable of imparting interrupted punch motion, resulting in enhanced room temperature formability. The exact mechanism of the formability improvement is not yet established. The contribution of interrupted motion in the ductility improvement has been studied through stress relaxation phenomena in uniaxial tensile (UT) tests. However, the reason for improved formability observed when employing servo press is complicated due to the additional contribution from frictional effects. In the present work, an attempt is made to decouple the friction effect on formability improvement numerically. The improved formability is studied using a hole expansion test (HET). The limit of forming during hole expansion is modeled using the Hosford–Coulomb (HC) damage criteria, which is implemented as a user subroutine in a commercial explicit finite element (FE) software. Only the contribution of stress relaxation is accounted for in the evolution of the damage variable during interrupted loading. Therefore, the difference between simulation and experimental hole expansion ratio (HER) can be used to decouple the friction effect from the overall formability improvement during hole expansion. The improvement in HER due to stress relaxation and friction effect is different. The study showed that the model effectively captures the hole expansion deformation process in both monotonic and interrupted loading conditions. Compared to stress relaxation, friction effect played a major role during interrupted HET.

Keywords: servo press; hole expansion test (HET); dual phase steel; finite element (FE) analysis; Hosford–Coulomb (HC) ductile fracture model

1 Introduction

Dual-phase (DP) steels, owing to their superior mechanical properties, are widely used in automotive applications [1–3]. However, poor stretch–flangeability is a concern associated with many advanced high strength steels (AHSS) including DP steels [4–6]. Stretch–flangeability, also referred to as edge formability, plays an important role in many sheet forming operations including bending and flanging. The hole expansion test (HET) is commonly used to measure the edge formability. In a standard HET, the blank with a center hole (CH) is expanded using a conical punch. The test is continuously monitored till the appearance of a through thickness crack, and the final diameter of the hole at fracture is measured. The ratio of the change in the hole diameter to the initial hole diameter is referred to as hole expansion ratio (HER). A large value of HER suggests higher edge formability. Generally, the CH of a standard HET

† Kali PRASAD and Aishwary GUPTA contributed equally to this work.

* Corresponding author: Kali PRASAD, E-mail: kali.iitm@gmail.com; Hariharan KRISHNASWAMY, E-mail: hariharan@iitm.ac.in

Nomenclature

a_m, b_m, c_m	Monotonic fracture parameters	ε_r	Strain ratio
a_r, b_r, c_r	Relaxation fracture parameters	ε_t	Thickness strain
d_f	Average final hole diameter	ε_{eq}	Equivalent strain
d_i	Average initial hole diameter	$\dot{\varepsilon}$	Strain rate
d_{outer}	Outer hole diameter at fracture	$\bar{\varepsilon}$	Equivalent plastic strain
d_{inner}	Inner hole diameter at fracture	$\bar{\varepsilon}_f$	Equivalent plastic strain at fracture
D_c	Damage variable	$\bar{\varepsilon}_r$	Equivalent plastic strain at relaxation
ΔD_c	Evolution of damage variable	η	Stress triaxiality
J_2	Second invariant of deviatoric stress tensor	μ	Friction coefficient
J_3	Third invariant of deviatoric stress tensor	$\bar{\theta}$	Lode angle parameter
k	Hardening law	σ_0	Initial yield stress (YS)
t	Relaxation time	σ_1, σ_2, σ_3	Principal stresses
t_i	Initial sheet thickness	σ_{vM}	Equivalent stress
t_{edge}	Sheet thickness around circumference at failure	$\bar{\sigma}_f$	Equivalent stress at fracture
ε	Strain at the beginning of relaxation	SDV1	Damage state variable : equivalent plastic strain
ε_1	Major strain		
ε_2	Minor strain	SDV3	Damage state variable : stress triaxiality
ε_c	Circumferential strain	SDV4	Damage state variable : Lode angle parameter
ε_p	Plastic strain		

specimen is prepared by punching process as it closely resembles the industrial practice. However, researchers [7–9] have also investigated other traditional machining processes like drilling, boring, wire cut electric discharge machining (W-EDM), and laser machining. It was experimentally shown that specimen prepared through W-EDM process yields the highest HER [8]. This trend was attributed to relatively very few defects with hole edge preparation from W-EDM process compared to those of other machining processes. It has been shown that in addition to the hole edge, strain path also plays a significant role in HER [10]. The influence of strain path on edge formability can be tested by varying the punch geometry [10, 11]. A conical punch would induce a uniaxial stress state, whereas a flat bottom punch subjects the specimen to a plane strain state in the vicinity of failure [11]. A hemispherical punch induces a complex and continuously varying strain path (stress state). Since plane strain state leads to early failure, it is expected that the HER estimated using a flat-bottomed punch would be less than that obtained by a conical punch, as reported by Pathak et al. [11], using dual phase and complex phase steels. Furthermore, the HER was also found to depend on several metallurgical factors such as material microstructure [1, 12], non-metallic inclusions [13], heat treatment condition [14, 15], alloy chemistry, [5] and relative strengths of the individual phases [4, 15].

Since the stress state is nearly uniaxial when deformed using a conical punch [3, 8, 11], attempts have been made to correlate uniaxial tensile (UT) properties with HER [16, 17]. It has been shown that yield strength (YS), ultimate tensile strength (UTS), uniform elongation (UE), etc., have a positive correlation with HER [17, 18]. Fang et al. [14] investigated the hole expansion behavior of C–Mn steels with different heat treatment conditions and concluded that HER increases with the ratio of YS/UTS. Recent studies indicate that HER correlates better with fracture toughness than tensile properties [6]. High HER is obtained in materials exhibiting higher fracture toughness. HER can be potentially improved if the onset of fracture can be delayed during plastic deformation. It has been shown that stress relaxation during plastic deformation delays the onset of fracture. This has been experimentally verified in many materials [19–24]. The improvement is primarily

attributed to the combined effect of dislocation annihilation and homogenization of internal stress [25–27]. During HET, intermittent stopping of the conical punch during deformation is expected to delay the onset of fracture due to stress relaxation and improve HER.

The first systematic study of interrupted HET was recently reported by Prasad et al. [9]. As expected, the HER evaluated during interrupted HET was much higher than the corresponding monotonic values. Interestingly, the strain increment to onset of fracture during HET in the above study was much higher than the ductility improvement observed during UT test at similar conditions. Since a conical punch was used, the difference was not due to any change in strain path①. The authors attributed the difference to the effect of friction on the interrupted behavior. The friction coefficient between punch and blank is influenced by several factors such as contact pressure, sliding velocity, material grade, lubrication, and temperature [29]. The magnitude of the friction coefficient influences the metal flow over the punch, determining the quality of the component being formed. The concept of friction coefficient is strictly applicable to Coloumb's adhesion friction law that assumes a linear relation between friction (shear) force and normal force. In typical sheet forming applications, the normal force is high, and the linearity of Coloumb's law is not adhered. Yet, most numerical simulations assume a constancy of friction coefficient. A common example on the role of friction in sheet forming can be demonstrated using a hemispherical punch test, where the location of failure is shifted from the pole due to friction [30–32]. The hemispherical punch test is used to establish the forming limit diagram (FLD), an accepted failure criterion to evaluate the formability [33]. Kim et al. [34] stamped AHSS by varying the lubrication condition and determined the critical interface pressure and temperature that leads to failure. In an interesting study, Stembalski et al. [35] estimated the friction coefficient to be inversely proportional to normal pressure and sliding velocity. Similar observations were reported in Refs. [36, 37]. Furthermore, analytical equations were proposed in this study to account for the influence of normal pressure and sliding velocity while estimating the friction coefficient. The aforesaid studies clearly show the importance of friction condition while forming sheet metal components.

In servo press forming, interrupted motion has been frequently employed to increase formability and decrease springback. During the interrupted motion, both normal pressure and velocity decrease. As discussed earlier, friction coefficient is sensitive to normal pressure and velocity [36, 37]. Therefore, it is likely that the friction coefficient varies during the interrupted motion, which influences the sheet formability. In addition to the friction effect, other components such as stress relaxation and change in strain path possibly play a crucial role in affecting the formability. Therefore, elucidating the underlying mechanism and decoupling and quantifying individual component contributions are essential for developing robust process models for sheet metal forming applications employing servo presses. Except for a recent work by Prasad et al. [9], no comprehensive investigations in this direction have been conducted.

In the present work, it is attempted to analyze the HER improvement during interrupted loading in the framework of continuum damage theory. The reason for using continuum damage model to analyze the intermittent HET is multifold, while the limiting strain of localized neck formation through forming limit diagram is commonly utilized to analyze sheet forming process, the failure in HET is by fracture, and the fracture strain exceeds the limiting strain. Besides, the edge cracking is strongly influenced by the edge preparation process (drilling, punching, etc.), which prevents the proposition of a correlation between the localized necking strain under the same strain path.

Extensive research has been done in the field of ductile fracture modeling, and various fracture models have been proposed. Earlier studies by McClintock [38], Rice and Tracy [39], Gurson [40], and Needleman and Tvergaard [41] focused primarily on the influence of hydrostatic stress on the void growth to predict ductile fracture. Based on this understanding, for tensile dominated loading, various triaxiality (η) based empirical formulations were proposed to model ductile damage [39, 43–45]. Chung et al. [45] used stress triaxiality based ductile fracture criterion to predict HER for three grades of AHSS. Butcher et al. [46] used Gurson–Tvergaard–Needleman (GTN) based damage model to describe the material behavior for DP600

① Changing the strain path during deformation can enhance the failure limit [28].

steel. Barnwal et al. [47] used triaxiality based ductile fracture criteria proposed by Rice and Tracey [39] to predict the onset of fracture in HET. It has been shown that damage models based only on triaxiality could not completely capture the damage behavior under shear dominant loading [48]. A more general fracture criteria was introduced by Xue and Wierzbicki [49] with the third stress invariant in the weighing function. Xue [44] established the influence of Lode angle parameter on the damage evolution of material and proposed a damage model based on both stress triaxiality and Lode angle parameter. Furthermore, recent fracture models, such as the model proposed by Bai and Wierzbiki [50], shear stress based modified Mohr–Coulomb model [51], and Hosford–Coulomb (HC) model [52] included the influence of stress triaxiality and Lode angle parameter in the numerical formulations. Recent comparative studies on ductile fracture models have shown that HC model shows better predictive capability for various loading conditions [53].

In the present work, analysis of HET using the HC damage model is extended to analyze the interrupted HET. The objective of the present work is to quantify the role of friction in HET. In the absence of friction effect, it is expected that the increment in fracture strain due to stress relaxation would be similar to that of UT test. Therefore, the contribution of fracture strain increment during HET is obtained by extrapolating the ductility improvement measured under uniaxial tension. The evolution of damage parameters is fit to model the ductility improvement during stress relaxation. The damage model thus obtained is used to predict the HER. The above methodology predicts only the contribution of viscoplastic effect on the HER improvement. The difference between the trend in experiment and simulation gives the role of friction in interrupted HER.

2 Materials and methods

DP600 steel with thickness = 2.6 mm obtained from ArcelorMittal① was studied. The UT and HET results are reported in Ref. [9]. The procedure and key results are summarized briefly for completeness. The uniaxial and stress relaxation tests were performed at a strain rate of 0.042 s^{-1}②. Two stress relaxation tests were performed by interrupting the deformation at 50% and 70% of UTS for a period of 60 s. Additional tensile tests were performed in specimens with different specimen geometries (Section 3.4). These experiments are performed to calibrate the fracture model.

The HET were conducted as per the International Standardization Organization (ISO) 16630:2017 standard [54] (Fig. 1). HET experiments were conducted in monotonic mode and interrupted loading condition. In the interrupted HET, the punch motion was interrupted for a duration of 60 s after reaching a certain pre-defined depth. During the holding period, the specimen was not unloaded. Detailed experimental procedure is mentioned in our recent work [9]. A schematic illustration of punch displacement for the two loading modes is schematically shown in Fig. 2. The test was continuously monitored through a camera, and the appearance of through thickness crack was used to stop the test. The HER value is calculated by Eq. (1):

$$\mathrm{HER} = \frac{d_\mathrm{f} - d_\mathrm{i}}{d_\mathrm{i}} \times 100\% \tag{1}$$

where d_f and d_i are the average final and initial hole diameters of the test specimen, respectively. Equivalent failure strain (ε_eq) during HET was estimated analytically by Eq. (2) following Butcher et al. [55]:

$$\begin{aligned} \varepsilon_\mathrm{eq} &= \frac{2}{3}(\varepsilon_\mathrm{c} - \varepsilon_\mathrm{t}) \\ \varepsilon_\mathrm{c} &= \ln\left(\frac{d_\mathrm{outer} + d_\mathrm{inner}}{2d_\mathrm{i}}\right) \\ \varepsilon_\mathrm{t} &= \ln\left(\frac{t_\mathrm{edge}}{t_\mathrm{i}}\right) \end{aligned} \tag{2}$$

where d_inner and d_outer refer to the inner and outer diameters at failure, respectively, t_i is the initial sheet thickness, and t_edge is the sheet thickness around the circumference at failure. ε_c and ε_t are circumferential and thickness strains, respectively. In this work, one

① Certain commercial equipment, instruments, software, or materials are identified to describe a procedure or concept adequately. Such identification is not intended to imply recommendation, endorsement, or implication by National Institute of Standards and Technology (NIST) that the equipment, instruments, software, or materials identified are necessarily the best available for the purpose.

② Corresponding to average strain rate during hole expansion test.

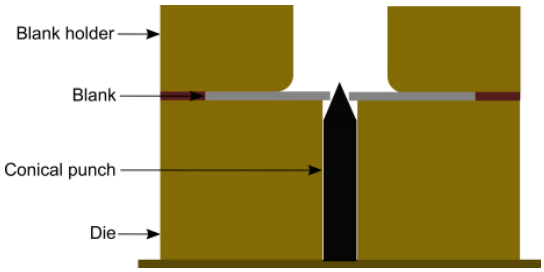

Fig. 1 Schematic representation of HET.

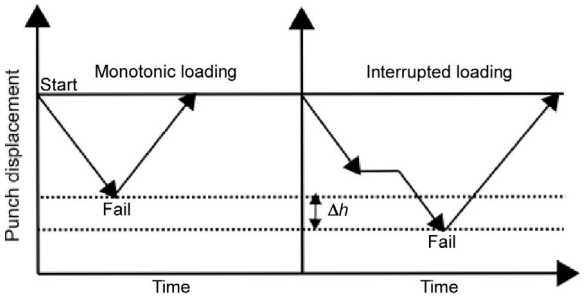

Fig. 2 Schematic diagram illustrating the punch travel in monotonic loading and interrupted loading (Δh indicates the additional depth formed during interrupted loading)

monotonic HET and two interrupted HETs were performed (50% and 70% of the monotonic punch displacement), and each interrupted HET was performed for 60 s holding time.

3 Constitutive modeling and calibration of ductile damage model

3.1 Plasticity and hardening model

In the present work, von Mises yield criteria is used along with associative flow rule and isotropic hardening, as given in Eqs. (3) and (4). The strain hardening behavior is modeled using the combined Swift and Voce hardening law, as given in Eq. (5).

$$f(\sigma, k) = \sigma_{\mathrm{vM}} - k = 0 \tag{3}$$

$$\sigma_{\mathrm{vM}} = \sqrt{\frac{3}{2}J_2} = \sqrt{\frac{1}{2}(\sigma_1-\sigma_2)^2 + (\sigma_2-\sigma_3)^2 + (\sigma_3-\sigma_1)^2} \tag{4}$$

$$k(\varepsilon_{\mathrm{p}}) = \sigma_0 + zK\varepsilon_{\mathrm{p}}^{n} + (1-z)C(1-\mathrm{e}^{-\alpha\varepsilon_{\mathrm{p}}}) \tag{5}$$

where J_2 is the second invariant of deviatoric stress tensor, σ_1, σ_2, and σ_3 ($\sigma_1 < \sigma_2 < \sigma_3$) are the principal stresses, σ_{vM} is the equivalent stress, σ_0 is the initial YS, ε_{p} is the plastic strain, C, α, K, n are material constants, and z ($0 \le z \le 1$) is the weight factor that is used to combine Swift and Voce hardening laws. The values of σ_0, z, K, n, C, and α are 400 MPa, 0.74, 623.5 MPa, 0.45, 640.7 MPa, and 34.65, respectively. These parameters were taken from Ref. [9].

3.2 Ductile fracture modeling

An arbitrary stress state can be represented using stress triaxiality (η) and Lode angle parameter ($\bar{\theta}$). Both η and $\bar{\theta}$ control the effect of stress state on void evolution. Stress triaxiality is the ratio of mean stress to the hydrostatic stress (Eq. (6)). The parameter controls the micro-void growth during ductile fracture. A lower value of stress triaxiality prevents the void growth, thus postponing the fracture. $\bar{\theta}$ is a function of the third invariant of the stress deviator (Eq. (7)). It is used to distinguish between the different shear stress states in three dimensions. The parameter accounts for the shape change of voids, which is dependent on the specific shear stress state.

$$\eta = \frac{\sigma_1+\sigma_2+\sigma_3}{3\sigma_{\mathrm{vM}}} \tag{6}$$

$$\bar{\theta} = 1 - \frac{2}{\pi}\cos^{-1}\left(\frac{27J_3}{2\bar{\sigma}_{\mathrm{vM}}}\right) \quad (-1 \le \bar{\theta} \le 1) \tag{7}$$

where J_3 is the devatoric third stress invariant. References [39, 43, 56–58] have been reported, defining the relationship between the fracture strain and stress state.

3.3 HC ductile fracture model

Mohr and Marcadet [52] proposed HC fracture criterion to model ductile fracture initiation for advanced high strength sheets under proportional loading. HC fracture model assumes localization of deformation in a narrow zone, and the localization criterion can be given as

$$\sigma_{\mathrm{HF}} + c(\sigma_1+\sigma_3) = b \tag{8}$$

where σ_{HF} is the Hosford stress, with

$$\sigma_{\mathrm{HF}} = \left\{\frac{1}{2}\left[(\sigma_1-\sigma_2)^a + (\sigma_2-\sigma_3)^a + (\sigma_1-\sigma_3)^a\right]\right\}^{\frac{1}{a}} \tag{9}$$

where a ($0 \le a \le 2$) is the Hosford exponent, and c ($0 < c \le 2$) and b ($b \ge 0$) are the material parameters proportional to the maximum shear stress on the deviatoric plane, which refer to cohesion and frictional terms, respectively [52]. For $a = 1$, the HC model reduces to Mohr–Coulomb model [52]. Using $\bar{\theta}$-dependent functions, Eqs. (10)–(12) can be obtained.

$$f_1[\bar{\theta}] = \frac{2}{3}\cos\left(\frac{\pi}{6}(1-\bar{\theta})\right) \tag{10}$$

$$f_2[\bar{\theta}] = \frac{2}{3}\cos\left(\frac{\pi}{6}(3+\bar{\theta})\right) \tag{11}$$

$$f_3[\bar{\theta}] = -\frac{2}{3}\cos\left(\frac{\pi}{6}(1+\bar{\theta})\right) \tag{12}$$

Using Eqs. (10)–(12) in Eq. (8), σ_{HF} can be written as

$$\sigma_{\mathrm{HF}} = \frac{b}{\left[\frac{1}{2}(f_1-f_2)^a + (f_2-f_3)^a + (f_1-f_3)^a\right]^{\frac{1}{a}} + c(2\eta + f_1 + f_3)} \tag{13}$$

Strain at onset of fracture ($\bar{\varepsilon}_{\mathrm{f}}$) is formulated by taking the inverse of hardening law $\bar{\varepsilon}_{\mathrm{f}} = k^{-1}\bar{\sigma}_{\mathrm{f}}$.

A damage variable (D_{c}) is introduced as a state variable given by Eq. (14):

$$D_{\mathrm{c}} = \int_0^{\bar{\varepsilon}_{\mathrm{f}}} \frac{\mathrm{d}\bar{\varepsilon}}{\bar{\varepsilon}_{\mathrm{f}}(\eta, \bar{\theta})} \tag{14}$$

where $\mathrm{d}\bar{\varepsilon}$ denotes the equivalent plastic strain increment. $D_{\mathrm{c}} = 1$ marks the onset of fracture, and the corresponding $\bar{\varepsilon}_{\mathrm{f}}$ is referred to as fracture strain. The use of damage variable ensures strain path dependence on the onset of fracture.

For damage modeling in case of stress relaxation, the fracture model is split into two parts, i.e., the onset of fracture surface before the stress relaxation point and the onset of fracture surface after the stress relaxation point. Two sets of parameters (a, b, c) need to be calibrated to denote the fracture surface with and without relaxation. Let $\bar{\varepsilon}_{\mathrm{r}}$ be the equivalent plastic strain, at which relaxation occurs. Then, for $\bar{\varepsilon}$ less than $\bar{\varepsilon}_{\mathrm{r}}$, the fracture model will be based on monotonic fracture parameters (a_{m}, b_{m}, and c_{m}); while for $\bar{\varepsilon}$ greater than or equal to $\bar{\varepsilon}_{\mathrm{r}}$, the fracture parameters will switch to relaxation fracture parameters (a_{r}, b_{r}, and c_{r}). Therefore, $\bar{\varepsilon}_{\mathrm{r}}$ may also be referred to as switching strain for the fracture surface. Thus, the evolution of D_{c} is modified according to Eq. (15) in case of stress relaxation.

$$D_{\mathrm{c}} = \int_0^{\bar{\varepsilon}_{\mathrm{f}}} \frac{\mathrm{d}\bar{\varepsilon}}{\bar{\varepsilon}_{\mathrm{f}}(\eta, \bar{\theta}, \bar{\varepsilon})} \tag{15}$$

where

$$\bar{\varepsilon}_{\mathrm{f}}(\eta, \bar{\theta}, \bar{\varepsilon}) = \begin{cases} \bar{\varepsilon}_{\mathrm{f}}(\eta, \bar{\theta}, a_{\mathrm{m}}, b_{\mathrm{m}}, c_{\mathrm{m}}) & (\bar{\varepsilon} < \bar{\varepsilon}_{\mathrm{r}}) \\ \bar{\varepsilon}_{\mathrm{f}}(\eta, \bar{\theta}, a_{\mathrm{r}}, b_{\mathrm{r}}, c_{\mathrm{r}}) & (\bar{\varepsilon} \ge \bar{\varepsilon}_{\mathrm{r}}) \end{cases}$$

3.4 Fracture tests and HC model calibration

To obtain the material parameters of the HC model, experimental fracture tests were performed over a wide range of stress states. The specimen geometries were chosen such that they provide a wide range of stress states. Four types of specimen geometry were chosen as UT, notch specimen (NT), CH, and in-plane shear specimen (SH), as shown in Fig. 3. Specimens were cut along the rolling direction of the sheet using W-EDM. Specimens were tested using a 100 kN universal tensile testing machine (Z100, Zwick/Roell) equipped with a video extensometer at a strain rate of 0.042 s^{-1}. All the experiments were repeated three times for statistical significance.

For calibration of HC damage parameters, finite element (FE) simulations were carried out for each specimen geometry. It is assumed that the location of the onset of fracture coincides with the location of the highest equivalent plastic strain in each specimen geometry. Thus, the critical element is selected at the location of the highest equivalent plastic strain, as shown in Fig. 4.

The loading history denoted by triaxiality $\eta_i(\varepsilon_{\mathrm{p}})$ and Lode angle parameter $\bar{\theta}_i(\varepsilon_{\mathrm{p}})$ of each calibration experiment (i.e., UT, SH, and NT) was evaluated with the help of FE simulation. The loading histories of critical element for each specimen geometry can be seen in Fig. 5. Let $\Omega = \{a, b, c\}$ be a set of calibration parameters that need to be optimized. The fracture strain $\bar{\varepsilon}_{\mathrm{f}}^i = \bar{\varepsilon}_{\mathrm{f}}^i(\Omega)$ for each loading case is calculated according to Eq. (16) to optimize the parameters in the fracture model.

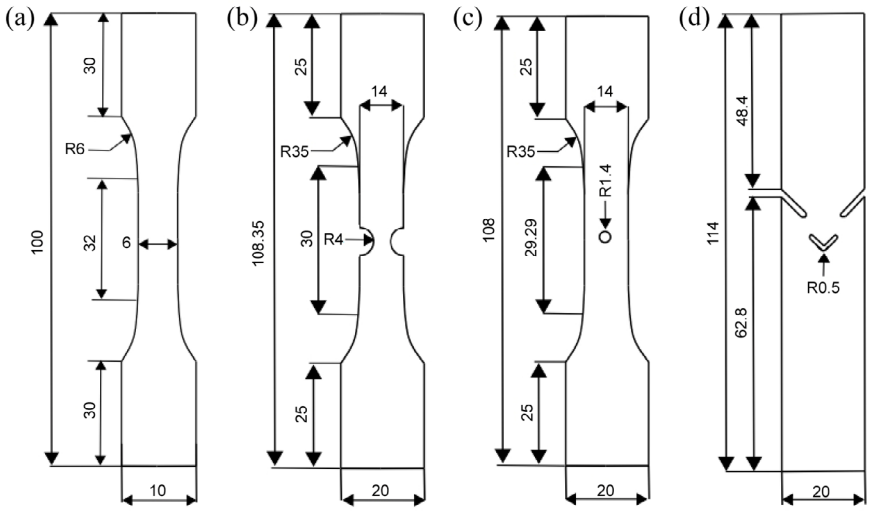

Fig. 3 Schematic of specimen geometries for (a) UT, (b) NT, (c) CH, and (d) SH specimens (all dimensions are in mm).

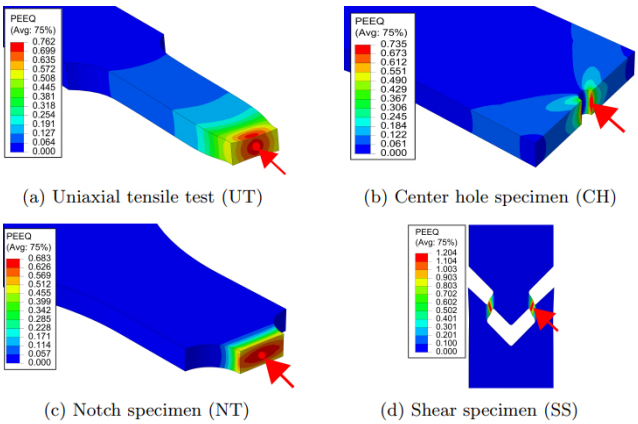

Fig. 4 Plastic strain distributions and locations of critical elements for (a) UT, (b) CH, (c) NT, and (d) SS specimens (the red dot marked symbol represents the location of critical element).

$$\int_0^{\bar{\varepsilon}_f} \frac{\mathrm{d}\bar{\varepsilon}}{\bar{\varepsilon}_f(\eta,\bar{\theta})} = 1 \tag{16}$$

The following minimization problem (Eq. (17)) is solved with the help of simplex algorithm using MATLAB code to obtain an optimized set of parameters $[\Omega]$ for the fracture model.

$$\Omega = \min_{\Omega} \sum_i \| \varepsilon_f^i[\Omega] - \varepsilon_{\exp}^i \| \quad \forall i \in [\mathrm{UT},\ \mathrm{SH},\ \mathrm{NT}] \tag{17}$$

where $\varepsilon_{\exp}^i$ is the equivalent plastic strain at the onset of fracture for the ith experiment.

The calibrated HC model parameters for monotonic case, i.e., a_m, b_m, and c_m are given in Table 1.

The ductility improvement due to stress relaxation is estimated from interrupted UT tests. The force–displacement data of the stress relaxation tests interrupted as 50% and 70% of UTS strain are shown in Fig. 6. The observed trend is in line with Refs. [19–21] on ductility improvement due to stress relaxation.

For the calibration of fracture parameters in case of relaxation, a similar approach is used with the help

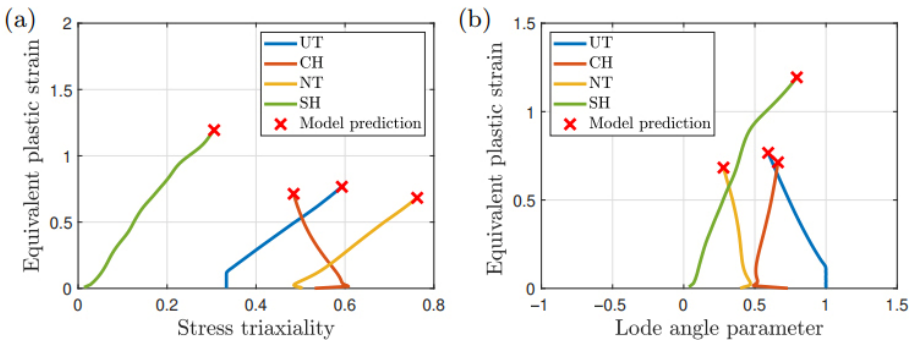

Fig. 5 Evolution of effective plastic strain as a function of (a) stress triaxiality and (b) Lode angle parameter. The red crosses represent the equivalent plastic strain values at the onset of fracture.

Table 1 Calibrated material parameters for HC fracture model for monotonic case.

Test mode	a_m	b_m	c_m
Monotonic	1.9	1,165	0.135

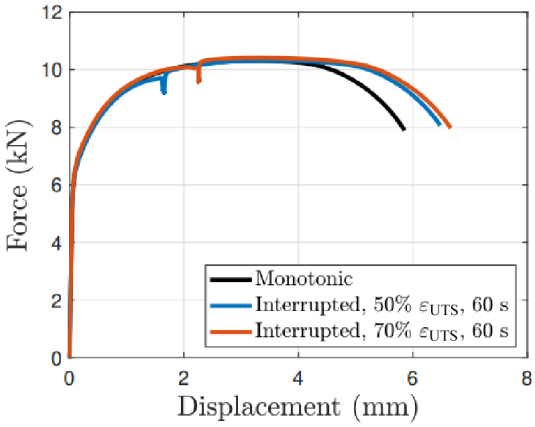

Fig. 6 Force–displacement curves for UT specimen subjected to monotonic and interrupted loading. Reproduced with permission from Ref. [9], © CIRP 2020.

of the obtained a_m, b_m, and c_m and plastic strain at the relaxation point, at which the model switches to a_r, b_r, and c_r. Then, similar to the monotonic case, the minimization problem is solved such that the predicted fracture strain according to the modified HC model coincides with the experimental fracture point for each of the relaxation cases, i.e., relaxation at 50% and 70% UTS. For the estimation of relaxation HC parameters for HET, the fracture strains for 50% and 70% punch travel relaxation points are estimated using the empirical equation of ductility improvement (Eq. (18)), which has been reported in the work of Prasad et al. [9].

$$\varepsilon_r = 1.22\varepsilon^{0.055}(\dot{\varepsilon} * t)^{0.0019} \tag{18}$$

where ε_r is the ratio of relaxation strain to monotonic strain, $\dot{\varepsilon}$ is the strain rate, t is the relaxation time, and ε is the strain at the beginning of relaxation. The strain at the start of relaxation was estimated using monotonic HET simulation for 50% and 70% punch travel. The HC model parameters were then calibrated following the procedure explained in Section 3.4.

It is to be noted that for simplicity, only parameter b in HC model is modified, and parameters a and c are assumed to be invariant during stress relaxation. The parameters a and c primarily control the shape of the fracture surface, whereas parameter b primarily controls the position of fracture surface in the z direction. The assumption of shape of fracture surface being the same in case of relaxation has been taken for simplicity. As the primary focus of this study is towards the application in HET, this assumption is acceptable as the loading history in case of HET is very similar to the uniaxial case.

The calibrated relaxation model parameters for the modified HC model with stress relaxation point, at which the monotonic model parameters are switched, are given in Table 2. ε_r for the HET is extrapolated using Eq. (18). The three-simensional (3D) fracture surfaces for different HC model parameters are shown in Fig. 7.

4 FE simulation

FE simulation of the specimens (Fig. 3) were performed with ABAQUS\Explicit 6.14 software. Three-dimensional continuum elements (C3D8R) were used to mesh the sheet specimens. Classical

Table 2 Calibrated material parameters for modified HC fracture model.

Test mode	Point of relaxation	Time (s)	a_r	b_r	c_r	$\bar{\varepsilon}_r$
UT	50% UTS	60	1.9	1,245	0.135	0.04411
UT	70% UTS	60	1.9	1,275	0.135	0.05987
Hole expansion	50% punch travel	60	1.9	1,442	0.135	0.22014
Hole expansion	70% punch travel	60	1.9	1,518	0.135	0.3346

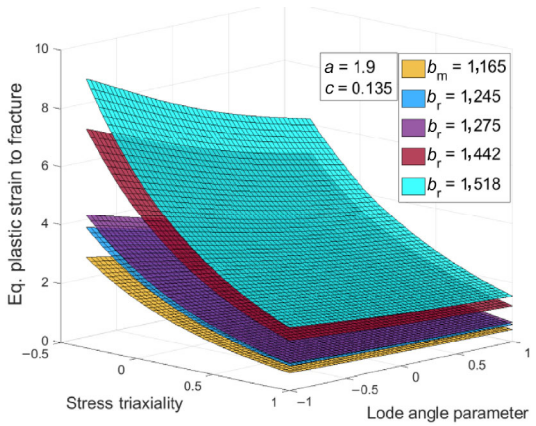

Fig. 7 Representation of fracture surfaces of HC model (in the above plot, $a = a_m = a_r = 1.9$, and $c = c_m = c_r = 0.135$).

isotropic hardening with von Mises criteria was used in the present FE analysis. An elasticity modulus of 200 GPa and a Poisson's ratio of 0.3 have used to model the elastic response of DP600 steel. The HC damage criteria was implemented as a user defined subroutine (VUMAT) in ABAQUS software (Fig. 8). The effective plastic strain, continuum damage variable stress triaxiality (η), and Lode angle parameter ($\bar{\theta}$) are defined as state variables in the VUMAT. The onset of fracture for each FE simulation is assumed when the damage variable reaches unity. The mesh size has been chosen based on a mesh sensitivity analysis; an element size of 0.1 mm was used near the critical region. Around ten through thickness elements have been chosen for each specimen geometry. FE simulation of HET was similar to that of UT specimen, with the difference only in the boundary conditions. In the case of HET simulation, the blank edges were completely constrained. The punch was restricted to move only in the vertical direction with a punch velocity of 10 mm/min. A friction coefficient of 0.2 was assumed to model the interaction at the tool blank interface.

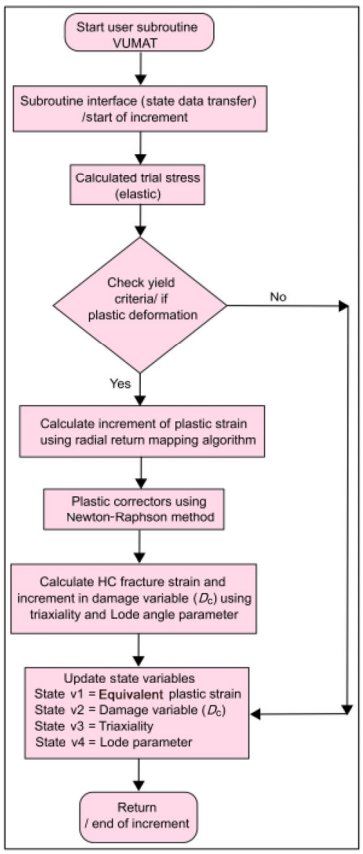

Fig. 8 Flow chart of VUMAT subroutine for HC fracture model.

5 Results and discussion

5.1 FE simulation of the fracture tests

As explained in Section 3.4, FE simulations for various specimen geometries were performed with the calibrated fracture model for monotonic case. The experimental and simulated force–displacement curves obtained from the fracture tests are shown in Figs. 9(a)–9(d). The onsets of fracture point are shown with red marks in Fig. 9. The representative plots show an excellent match between experimental and simulated data. This confirms the accuracy of the calibrated model for the investigated stress states.

For UT specimen, FE simulations were performed with the modified HC model for stress relaxation at 50% and 70% UTS strain. The parameters of HC model were switched at the point of relaxation, as explained in Section 3.3. Figure 10 shows the onset of fracture for the three cases of UT testing.

5.2 HET results

To comprehend the hole expansion deformation process, FE simulation of HET was performed. Figure 11(a) shows the distribution of stress triaxiality for HET specimen. The stress triaxility values near the hole edge are in the range of ~0.33–0.37, which nearly corresponds to the uniaxial stress state condition.

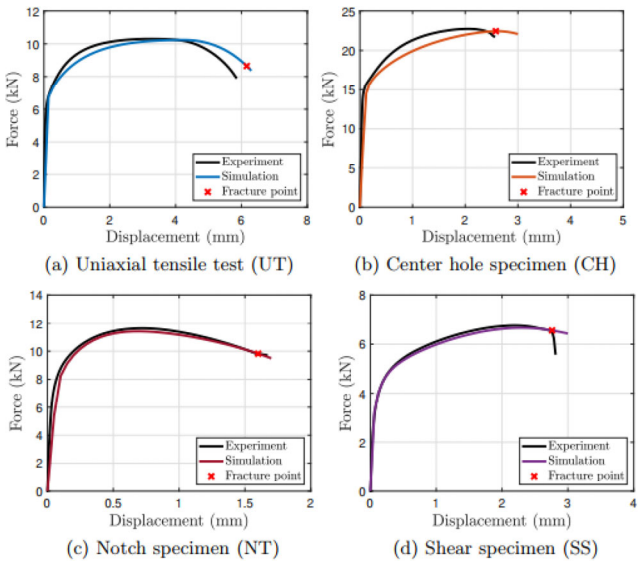

Fig. 9 Comparison of experimental and FE simulated force–displacement data for (a) UT, (b) CH, (c) NT, and (d) SS specimen (the red color marked symbols represent the onset of fracture).

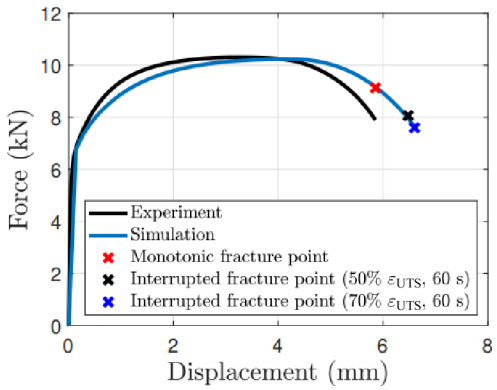

Fig. 10 Force–displacement of UT specimen. Reproduced with permission from Ref. [9], © CIRP 2020.

Figures 11(b) and 11(c) show the distributions of equivalent plastic strain and Lode angle parameter. From this distribution, it is concluded that the deformation in HET is primarily concentrated near the hole edge, and it nearly deforms in uniaxial stress condition. Figures 12(a)–12(f) show the comparison of experimental and simulated deformed HET specimens as well as contours of damage state variable (SDV2). It can be seen that the damage variable has a maximum value at the outer hole edge, where the onset of fracture occurs. Moreover, to evaluate the stress state at the hole edge, three elements viz. outer, middle, and inner edge along the through thickness direction were chosen. The major (ε_1) and minor strains (ε_2) corresponding to these respective elements were estimated and superposed in the strain path corresponding to the uniaxial stress state for isotropic

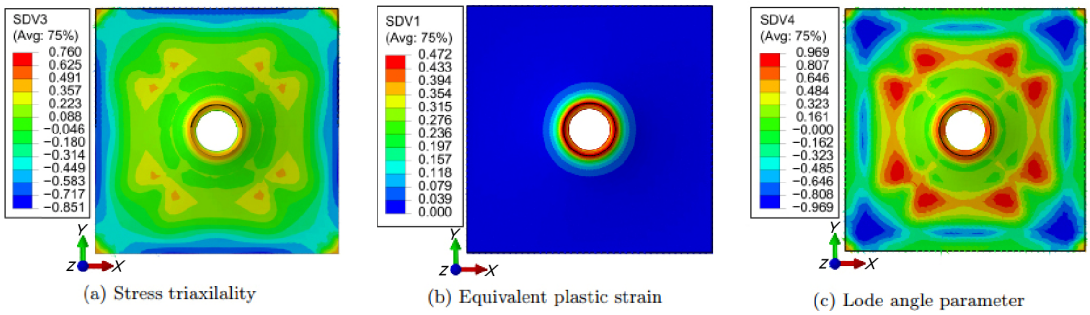

Fig. 11 FE simulation of hole expansion: distributions of (a) stress triaxiality, (b) equivalent plastic strain, and (c) Lode angle parameter.

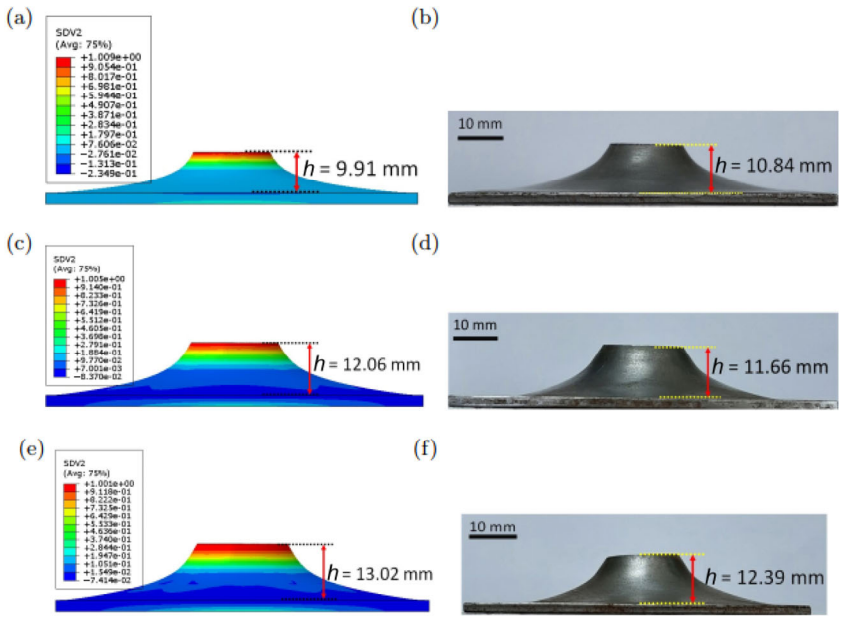

Fig. 12 Comparison of deformed HET specimen at the point of fracture. (a) Finite element method (FEM): monotonically, (b) experiment: monotonically, (c) FEM: interrupted loading at 50% punch travel, (d) experiment: interrupted loading at 50% punch travel, (e) FEM: interrupted loading at 70% punch travel, and (f) experiment: interrupted loading at 70% punch travel for 60 s.

material given by ($\varepsilon_1 = -2\varepsilon_2$), as shown in Fig. 13(a). It is observed that the outer and middle edge deforms nearly in an uniaxial stress state. However, the inner edge deviates from the uniaxial stress state. This deviation is possibly due to the compressive stress and friction condition between the sheet and conical punch.

Figure 13(b) shows the major (ε_1) and minor strains (ε_2) in the outer edge element. In Fig. 13(b), the respective "×" symbol refers to the major and minor strains for monotonic and interrupted loading conditions at fracture, estimated using experiment and FE analysis. The fracture points shifts when the specimen was subjected to interrupted loading.

Figure 14 shows the evolution of the HC damage variables with punch displacement in monotonic and interrupted HET. The fracture is assumed to initiate when damage variable reaches to unity. It is to be noted that during monotonic HET, the damage variable monotonically increases with punch displacement, and the specimen fails at comparatively less failure strain. However, in interrupted HET, the specimens underwent larger failure strain before the initiation of fracture, which is manifested by delay in the saturation of damage variable.

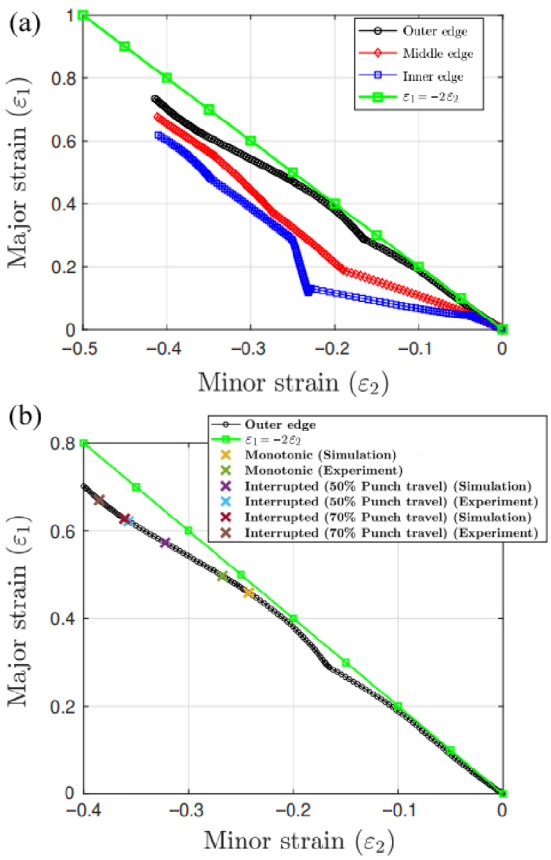

Fig. 13 (a) Strain path evolution during HET and (b) major (ε_1) and minor strains (ε_2) at fracture in monotonic and interrupted loading conditions in the outer edge.

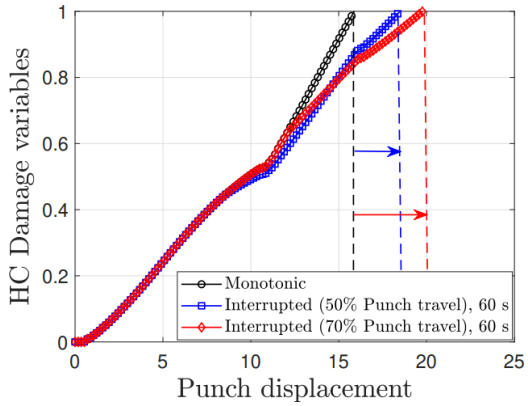

Fig. 14 Evolution of HC damage variables in monotonic and interrupted HET with punch displacement (the respective arrows indicate the delay in damage variables due to interrupted loading).

The HERs were estimated by Eq. (1). Figures 15(a) and 15(b) show the comparison of experimental and simulated HER values and corresponding fracture strains for monotonic loading condition. It is observed that experimental HER and fracture strain are higher than those of predicted through FE analysis. This difference is attributed to the definition of failure or fracture in experiment and FE analysis. In FE analysis, the failure is considered when the damage variable saturates to unity. The FE analysis accounts only for the initiation of fracture, and the evolution of fracture was not taken into consideration, whereas in experiment, the HER values were estimated once the through thickness crack appears. This accounts for both damage initiation and propagation. Additionally, uncertainty associated with the detection of through thickness crack also poses an experimental challenge to accurately estimate the HER and fracture strain. Due to this, the experimental values were higher than those of predicted data.

To further understand the effect of interrupted loading in HET, the experimental and simulated HER values and their corresponding fracture strains are shown in Figs. 16(a) and 16(b), respectively. On comparing with those of monotonic loading condition (Figs. 15(a) and 15(b)), it is observed that interrupted HET has resulted into higher values of HER and fracture strains. This improvement was found to depend on punch travel. Moreover, the increment in

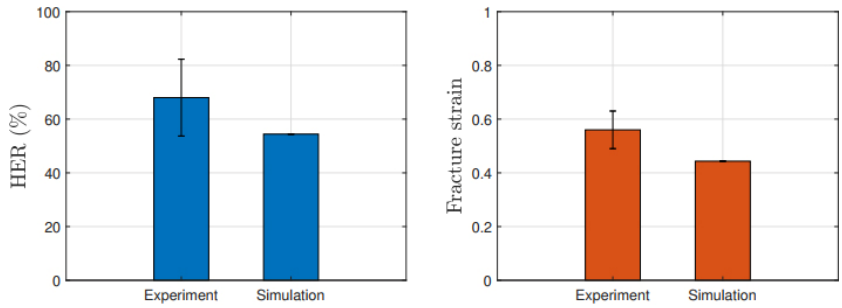

(a) HER (%) (b) Fracture strain

Fig. 15 Comparison of experimental and simulated (a) HER values and (b) fracture strains for monotonic loading condition. Reproduced with permission from Ref. [9], © CIRP 2020.

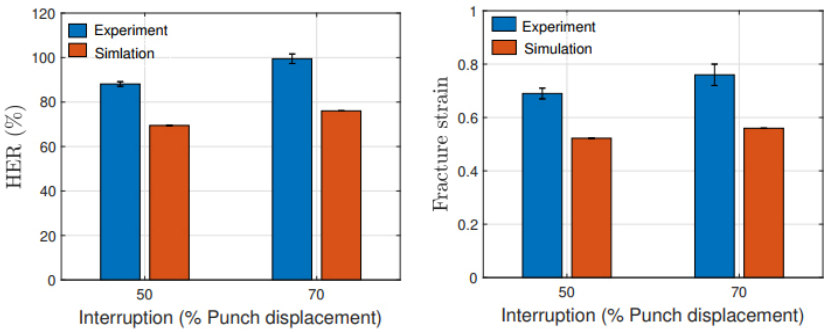

(a) HER (%) (b) Fracture strain

Fig. 16 Comparison of experimental and simulated (a) HER values and (b) fracture strains for interrupted loading conditions. Reproduced with permission from Ref. [9], © CIRP 2020.

HER and corresponding fracture strain was much higher in experiment compared to that in the simulated value. Since the interrupted HET experiments were performed without unloading the specimens, as explained earlier in Section 2, the samples were subjected to stress relaxation phenomena. In addition to stress relaxation, elastic recovery during relaxation also alters the contact stresses and contact areas between punch and blank. This influences the mechanical behavior of the specimen during interrupted HET by changing the pressure-dependent friction coefficient [59, 60]. However, the simulated HET accounts only for the stress relaxation effect, which is due to the viscoplastic effect of the material. Therefore, the difference in trend between the experimental and predicted values will give the net contribution of improvement predominantly due to friction effect.

The contributions of stress relaxation and friction effect in interrupted HET are quantified using a parameter ($\Delta H = \frac{\mathrm{HER_I} - \mathrm{HER_M}}{\mathrm{HER_M}}$), where $\mathrm{HER_I}$ and $\mathrm{HER_M}$ refer to the interrupted and monotonic HER using experimental and simulated values, respectively. Figure 17 shows the comparison of parameter ΔH with punch displacement at interruption. It is observed that ΔH monotonically increases with punch displacement at interruption. The slopes of the experimental and simulated ΔH are 0.0065 and 0.0056, respectively. The ΔH for experiment captures both stress relaxation and friction effect, whereas ΔH

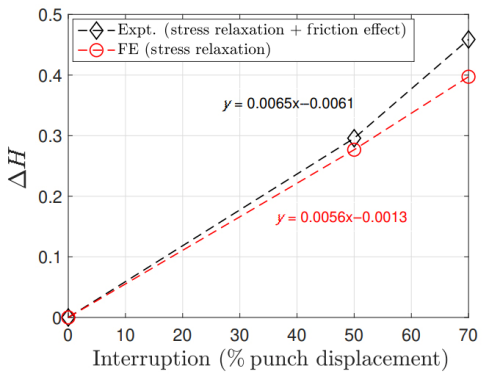

Fig. 17 Comparison of friction and stress relaxation effect in interrupted HET (the functions represent the trendline of the data points).

for simulation captures only the effect of stress relaxation. The difference in the slope is attributed purely due to friction effect. It is important to note that the contribution of friction effect increases with the punch displacement at interruption. This explains the formability improvement in interrupted HET when the interruption was performed at higher punch travel. In order to account this friction effect in simulation, the evolution of damage variable should be made a function of μ, i.e., presently $\Delta D_c = f(\sigma, \varepsilon, t)$, and proposed $\Delta D_c = f(\sigma, \varepsilon, t, \mu)$. Further systematic studies are required to obtain the evolution of damage variable as a function of interface friction.

6 Conclusions

The present study investigates the effect of monotonic and interrupted loading on the hole expansion deformation behavior of DP600 steel. A comprehensive FE analysis of HET was performed, and HC ductile damage model was implemented in the FE model. It is observed that the FE model effectively captures the hole expansion deformation process in both monotonic and interrupted loading conditions. Compared to those of monotonic loading condition, higher values of HER and fracture strains were observed in interrupted HET. The overall improvement in HER was primarily due to the two concurring effects, namely stress relaxation and friction effect. The friction was found to play a major role compared to stress relaxation in improving HER during interrupted HET.

Acknowledgements

The authors would like to express their gratitude to ArcelorMittal for providing the steel utilized in this study. Authors affiliated to Indian Institute of Technology Madras gratefully acknowledge the funding received from the Institute of Eminence Research Initiative project on materials and manufacturing for futuristic mobility.

Declaration of competing interest

The authors have no competing interests to declare that are relevant to the content of this article.

References

[1] Calcagnotto M, Ponge D, Raabe D. Effect of grain refinement to 1 μm on strength and toughness of dual-phase steels. *Mater Sci Eng A* **527**(29–30): 7832–7840 (2010)

[2] Qu H, Michal G M, Heuer A H. A 3rd generation advanced high-strength steel (AHSS) produced by dual stabilization heat treatment (DSHT). *Metall Mater Trans A* **44**(10): 4450–4453 (2013)

[3] Prasad K, Krishnaswamy H, Banerjee D, Chakkingal U. An investigation into the influence of interrupted loading in improving the stretch–flangeability of dual phase steel. *Defect and Diffusion Forum* **414**: 81–87 (2022)

[4] Hasegawa K, Kawamura K, Urabe T, Hosoya Y. Effects of microstructure on stretch–flange–formability of 980 MPa grade cold-rolled ultra high strength steel sheets. *ISIJ Int* **44**(3): 603–609 (2004)

[5] Lee J, Lee S J, de Cooman B C. Effect of micro-alloying elements on the stretch–flangeability of dual phase steel. *Mater Sci Eng A* **536**: 231–238 (2012)

[6] Yoon J I, Jung J, Joo S H, Song T J, Chin K G, Seo M H, Kim S J, Lee H, Kim H S. Correlation between fracture toughness and stretch–flangeability of advanced high strength steels. *Mater Lett* **180**: 322–326 (2016)

[7] Paul S K, Mukherjee M, Kundu S, Chandra S. Prediction of hole expansion ratio for automotive grade steels. *Comput Mater Sci* **89**: 189–197 (2014)

[8] Paul S K. A critical review on hole expansion ratio. *Materialia* **9**: 100566 (2020)

[9] Prasad K, Venkatesh B, Krishnaswamy H, Banerjee D K, Chakkingal, U. On the interplay of friction and stress relaxation to improve stretch–flangeability of dual phase (DP600) steel. *CIRP J Manuf Sci Tec* **32**: 154–169 (2021)

[10] Paul S K. Effect of punch geometry on hole expansion ratio. *P I Mech Eng B-J Eng* **234**(3): 671–676 (2020)

[11] Pathak N, Butcher C, Worswick M J. Experimental techniques for finite shear strain measurement within two advanced high strength steels. *Exp Mech* **59**(2): 125–148 (2019)

[12] Yoon J I, Lee H H, Jung J, Kim H S. Effect of grain size on stretch–flangeability of twinning-induced plasticity steels. *Mater Sci Eng A* **735**: 295–301 (2018)

[13] Mandal G K, Ashok K, Das S K, Biswas P, Sarkar R B, Sundara Bharathy R, Srivastava V C. Development of stretch flangeable grade steels by inclusion engineering approach. *J Mater Eng Perform* **27**(11): 5622–5634 (2018)

[14] Fang X, Fan Z, Ralph B, Evans P, Underhill R. The relationships between tensile properties and hole expansion property of C–Mn steels. *J Mater Sci* **38**: 3877–3882 (2003)

[15] Fang X, Fan Z, Ralph B, Evans P, Underhill R. Effects

of tempering temperature on tensile and hole expansion properties of a C–Mn steel. *J Mater Process Technol* **132**(1–3): 215–218 (2003)

[16] Sadagopan S, Urban D, Wong C, Huang M, Yan B D. Formability characterization of a new generation high strength steels. In: Proceedings of the Office of Scientific and Technical Information (OSTI), Pittsburgh, USA, 2003: 0012.

[17] Paul S K. Non-linear correlation between uniaxial tensile properties and shear-edge hole expansion ratio. *J Mater Eng Perform* **23**(10): 3610–3619 (2014)

[18] Prasad K, Ebrahim A S, Krishnaswamy H, Chakkingal U, Banerjee D K. Evaluation of hole expansion formability of high strength AA7075 alloy under varying temper conditions. *IOP Conf Ser Mater Sci Eng* **1238**(1): 012038 (2022)

[19] Hariharan K, Majidi O, Kim C, Lee M G, Barlat F. Stress relaxation and its effect on tensile deformation of steels. *Mater Design* **52**: 284–288 (2013)

[20] Hariharan K, Dubey P, Jain J. Time dependent ductility improvement of stainless steel SS 316 using stress relaxation. *Mater Sci Eng A* **673**: 250–256 (2016)

[21] Prasad K, Krishnaswamy H, Jain J. Leveraging transient mechanical effects during stress relaxation for ductility improvement in aluminium AA 8011 alloy. *J Mater Process Technol* **255**: 1–7 (2018)

[22] Prasad K, Krishnaswamy H, Arunachalam N. Investigations on ductility improvement and reloading yielding during stress relaxation of dual phase Ti–6Al–4V titanium alloy. *J Alloys Compd* **828**: 154450 (2020)

[23] Li X F, Li J J, Ding W, Zhao S J, Chen J. Stress relaxation in tensile deformation of 304 stainless steel. *J Mater Eng Perform* **26**(2): 630–635 (2017)

[24] Prasad K, Krishnaswamy H, Banerjee D K. Experimental and modeling studies on the stress relaxation behaviour of Ti–6Al–4V alloy. In: Proceedings of the ASME 2021 Gas Turbine India Conference, Chennai, India, 2021.

[25] Varma A, Gokhale A, Jain J, Hariharan K, Cizek P, Barnett M. Investigation of stress relaxation mechanisms for ductility improvement in SS316L. *Philos Mag* **98**(3): 165–181 (2018)

[26] Lee H, Chae H, Kim Y S, Song M J, Lim S, Prasad K, Krishnaswamy H, Jain J, An K, Lee S Y. Viscoplastic lattice strain during repeated relaxation of age-hardened Al alloy. *Mech Mater* **158**: 103899 (2021)

[27] Prasad K, Balaji V, Krishnaswamy H, Phani P S, Carlone P. Rigorous analysis and pragmatic guidelines in estimating strain rate sensitivity using stress relaxation test. *Mech Mater* **168**: 104279 (2022)

[28] Stoughton T B. A general forming limit criterion for sheet metal forming. *Int J Mech Sci* **42**(1): 1–27 (2000)

[29] Folle L F, dos Santos Silva B C, Batalha G F, Coelho R S. The role of friction on metal forming processes. In: *Tribology of Machine Elements*. Pintaude G, Cousseau T, Rudawska A, Eds. Rijeka (Croatia): IntechOpen, 2022.

[30] Hariharan K, Prakash R V, Prasad M S. Influence of yield criteria in the prediction of strain distribution and residual stress distribution in sheet metal formability analysis for a commercial steel. *Mater Manuf Process* **25**(8): 828–836 (2010)

[31] Manikandan G, Verma R K, Biswas P. Effect of friction in stretch forming and its influence on the forming limit curve. *P I Mech Eng B-J Eng* **229**(6): 973–981 (2015)

[32] Rees D W A. Factors influencing the FLD of automotive sheet metal. *J Mater Process Technol* **118**(1–3): 1–8 (2001)

[33] Paul S K. Prediction of complete forming limit diagram from tensile properties of various steel sheets by a nonlinear regression based approach. *J Manuf Process* **23**: 192–200 (2016)

[34] Kim H, Han S, Yan Q, Altan T. Evaluation of tool materials, coatings and lubricants in forming galvanized advanced high strength steels (AHSS). *CIRP Ann* **57**(1): 299–304 (2008)

[35] Stembalski M, Preś P, Skoczyński W. Determination of the friction coefficient as a function of sliding speed and normal pressure for steel C45 and steel 40HM. *Arch Civ Mech Eng* **13**(4): 444–448 (2013)

[36] Azushima A, Kudo H. Direct observation of contact behaviour to interpret the pressure dependence of the coefficient of friction in sheet metal forming. *CIRP Ann* **44**(1): 209–212 (1995)

[37] Kim C, Lee J U, Barlat F, Lee M G. Frictional behaviors of a mild steel and a TRIP780 steel under a wide range of contact stress and sliding speed. *J Tribol* **136**(2): 021606 (2014)

[38] McClintock F A. A criterion for ductile fracture by the growth of holes. *J Appl Mech* **35**(2), 363–371 (1968)

[39] Rice J R, Tracey D M. On the ductile enlargement of voids in triaxial stress fields. *J Mech Phys Solids* **17**(3): 201–217 (1969)

[40] Gurson A L. Plastic flow and fracture behavior of ductile materials incorporating void nucleation, growth and interaction. Ph. D. Thesis. Providence (USA): Brown University, 1975.

[41] Needleman A, Tvergaard V. An analysis of ductile rupture in notched bars. *J Mech Phys Solids* **32**(6): 461–490 (1984)

[42] Johnson G R, Cook W H. Fracture characteristics of three metals subjected to various strains, strain rates, temperatures and pressures. *Eng Fract Mech* **21**(1): 31–48 (1985)

[43] Bao Y B, Wierzbicki T. On fracture locus in the equivalent strain and stress triaxiality space. *Int J Mech Sci* **46**(1): 81–98 (2004)

[44] Xue L. Damage accumulation and fracture initiation in uncracked ductile solids subject to triaxial loading. *Int J Solids Struct* **44**(16): 5163–5181 (2007)

[45] Chung K, Ma N, Park T, Kim D, Yoo D, Kim C. A modified damage model for advanced high strength steel sheets. *Int J Plast* **27**(10): 1485–1511 (2011)

[46] Butcher C, Anderson D, Worswick M. Predicting failure during sheared edge stretching using a damage-based model for the shear-affected zone. *SAE Int J Mater Manuf* **6**(2): 304–312 (2013)

[47] Barnwal V K, Lee S Y, Yoon S Y, Kim J H, Barlat F. Fracture characteristics of advanced high strength steels during hole expansion test. *Int J Fract* **224**(2): 217–233 (2020)

[48] Bouchard P O, Bourgeon L, Fayolle S, Mocellin K. An enhanced Lemaitre model formulation for materials processing damage computation. *Int J Mater Form* **4**(3): 299–315 (2011)

[49] Xue L, Wierzbicki T. Ductile fracture characterization of aluminium alloy 2024-T351 using damage plasticity theory. *Int J Appl Mechanics* **1**(2): 267–304 (2009)

[50] Bai Y L, Wierzbicki T. A new model of metal plasticity and fracture with pressure and Lode dependence. *Int J Plast* **24**(6): 1071–1096 (2008)

[51] Pack K, Mohr D. Combined necking & fracture model to predict ductile failure with shell finite elements. *Eng Fract Mech* **182**: 32–51 (2017)

[52] Mohr D, Marcadet S J. Micromechanically-motivated phenomenological Hosford–Coulomb model for predicting ductile fracture initiation at low stress triaxialities. *Int J Solids Struct* **67–68**: 40–55 (2015)

[53] Bharti S, Gupta A, Krishnaswamy H, Panigrahi S K, Lee M G. Evaluation of uncoupled ductile damage models for fracture prediction in incremental sheet metal forming. *CIRP J Manuf Sci Tec* **37**: 499–517 (2022)

[54] ISO 16630 2017 Metallic materials—Sheet and strip—Hole expanding test. ISO, 2017.

[55] Butcher C, Anderson D, Worswick M. Predicting failure during sheared edge stretching using a damage-based model for the shear-affected zone. *SAE Int J Mater Manf* **6**(2): 304–312 (2013)

[56] Rice J R. Mechanics of crack tip deformation and extension by fatigue. http://esag.harvard.edu/rice/013_Rice_MechCrackTipDefFatigue_ASTM67.pdf (1967)

[57] Rice J R, Rosengren G F. Plane strain deformation near a crack tip in a power-law hardening material. *J Mech Phys Solids* **16**(1): 1–12 (1968)

[58] Gurson A L. Continuum theory of ductile rupture by void nucleation and growth: Part I—Yield criteria and flow rules for porous ductile media. *J Eng Mater Technol* **99**(1): 2–15 (1977)

[59] Ma X, de Rooij M, Schipper D. A load dependent friction model for fully plastic contact conditions. *Wear* **269**(11–12): 790–796 (2010)

[60] Gil I, Mendiguren J, Galdos L, Mugarra E, de Argandoña E S. Influence of the pressure dependent coefficient of friction on deep drawing springback predictions. *Tribol Int* **103**: 266–273 (2016)

Kali PRASAD. He is currently a Ph.D. student in the Department of Mechanical Engineering at Indian Institute of Technology Madras, India. He received his master's degree in the Department of Metallurgical and Materials Engineering, Indian Institute of Technology Madras, India. His research interests mainly focus on the sheet metal forming and mechanical behaviour of materials.

Aishwary GUPTA. He is currently a Ph.D. student in the Department of Materials Science and Engineering, Seoul National University, Republic of Korea. He received his bachelor's and master's degrees in the Department of Mechanical Engineering, Indian Institute of Technology Madras, India. His research interests mainly focus on the ductile fracture modelling of metallic materials.

Hariharan KRISHNASWAMY. He is an associate professor in the Department of Mechanical Engineering at Indian Institute of Technology (IIT) Madras, India. Previously, he worked as an assistant professor at IIT Madras during 2016–2021. Prior to joining IIT Madras, he was an assistant professor in the Department of Mechanical Engineering at IIT Delhi. He received his Ph.D. from IIT Madras in 2012 and B.E. from University of Madras. Earlier, he has worked as a post-doc researcher in Graduate Institute of Ferrous Technology (GIFT), Pohang University of Science and Technology (POSTECH), Republic of Korea (2012–2014), and in the Research Department of Ashok Leyland Ltd, India (2004–2012). His research interests mainly focus on sheet metal forming, plasticity, fatigue, and mechanical behaviour of materials.

Dilip K. BANERJEE. He is a research engineer in the Mechanical Performance Group of the Materials Science and Engineering Division (MSED) of the Material Measurement Laboratory (MML) at the National Institute of Standards and Technology (NIST), USA. He received his B.Tech. degree (honours) from the Indian Institute of Technology Kharagpur, India, and his M.S. and Ph.D. degrees from The University of Alabama, USA, in materials engineering (an interdisciplinary program among Materials Engineering, Mechanical Engineering, and Engineering Mechanics Departments). His current research efforts are focused on developing accurate computational models in support of the NIST Center of Automotive Lightweighting (NCAL)'s goals to develop the measurement methodology and analysis necessary for the automotive industry to transition to advanced lightweighing materials and adopt these emerging materials as sheet metal components.

Uday CHAKKINGAL. He is a professor in the Department of Metallurgical and Materials Engineering at Indian Institute of Technology Madras, India. He received his Ph.D. from Rensselaer Polytechnic Institute, USA, in 1994. His research interests mainly focus on metal forming processes, sheet metal forming, severe plastic deformation processes, and aluminium, magnesium, titanium alloys and metallic biomaterials.

Myoung-Gyu LEE. He is a professor in the Department of Materials Science and Engineering at Seoul National University, Republic of Korea. He received his Ph.D. from Seoul National University, Republic of Korea, in 2004. Prior to joining Seoul National University, he was an associate professor in the Department of Material Science Engineering at Korea University, Republic of Korea. His research interests mainly focus on computational materials science, mechanics of materials, mechanics of anisotropic structure materials, experimental mechanics, optimization of manufacturing process, and forming and shaping of automotive parts.